Joint Special Interest Group meeting between euspen and ASPE
Advancing Precision in Additive Manufacturing
Inspire AG, St. Gallen, Switzerland 2021
www.euspen.eu

High-resolution X-ray computed tomography for additive manufacturing: Towards traceable porosity defect measurements using digital twins

B. A. Bircher[1], S. Wyss[1], D. Gage[2], A. Küng[1], C. Körner[2], F. Meli[1]

[1]Laboratory for Length, Nano- and Microtechnology, Federal Institute of Metrology METAS, Bern-Wabern, Switzerland
[2]Chair of Materials Science and Engineering for Metals, Friedrich-Alexander University Erlangen-Nürnberg, Erlangen, Germany

benjamin.bircher@metas.ch, felix.meli@metas.ch

Abstract

Metal additively manufactured (AM) parts pose new challenges for dimensional metrology due to their high surface roughness, buried structures and internal defects. X-ray computed tomography (XCT) is a powerful volumetric measurement method providing resolutions down to the micrometre level that enables us to address several quality assurance requirements simultaneously. It can accompany the entire AM process by being employed for AM powder characterisation, as a non-destructive testing (NDT) tool to characterise defects, such as porosity and unfused layers, and to assess the part geometry, for example by comparison to the nominal CAD model.
We will discuss the potential and limitations of XCT for metal AM and present a new approach to render classical NDT analyses, such as porosity, metrologically traceable by assigning a measurement uncertainty to them. The approach uses dedicated simulations of digital porosity representations, i.e. digital twins, as a route towards estimating the measurement uncertainty (MU) of the pore parameters, such as size and shape factors, and the probability of detection (POD) with respect to defect size.

X-ray computed tomography (XCT), additive manufacturing (AM), defects, porosity, dimensional metrology, measurement uncertainty (MU), probability of detection (POD), electron beam melting (EBM)

1. Introduction

Additive manufacturing (AM) is becoming increasingly important because of its key advantage for rapid prototyping, freedom of design, and sustainability. Due to the complex manufacturing process, metrology tools for quality assurance and dimensional analyses are essential [1]. X-ray computed tomography (XCT) is a promising modality thanks to its ability to map the complete inner and outer structure of parts [2]. However, there is still limited comparability for certain analyses, such internal defects [3] and surface texture [4].

Traceability that enables comparability entails introducing a reference scale and assigning a task specific measurement uncertainty. Whereas, the former was addressed for high-magnification measurements [5,6], uncertainty estimations for porosity measurements were only established using the substitution method [7]. This method is time consuming due to the required reference measurements and difficult to implement for internal features. Further, the strict similarity requirement between the reference object and the workpiece, according to VDI/VDE 2630-2.1 [8], prevents generalisability. Digital representations, i.e. virtual reference samples [9], are a promising approach to estimate uncertainties and in a future step correct for systematic deviations introduced by the measurement system itself.

In this paper, we present a route to render XCT porosity measurements traceable using dedicated simulations of digital porosity representations. According to references [10,11], a digital representation that feeds back information to the measurement result is referred to as "digital twin". This definition applies to the digital porosity representation here, since it aids the estimation of the measurement uncertainty.

2. Porosity simulations

Since traceability in XCT is still not fully established, it is of paramount importance to understand the complex nature of the measurement process to estimate a feature specific measurement uncertainty (MU) as well as a probability of detection (POS) in dependence of defect size. Simulations are a promising method to fully describe the XCT measurement process [12] and evaluate different analysis algorithms.

2.1. Digital porosity representation

Virtual reference samples were previously used to evaluate the performance of XCT for surface texture measurements [9] or to determine the probability of detection (POD) of defects in radiography [13].

We used the Python API in FreeCAD (Version 0.17.13522, www.freecadweb.org) to generate a cylindrical sample that was filled with spherical pore defects as follows (Figure 1): The radii

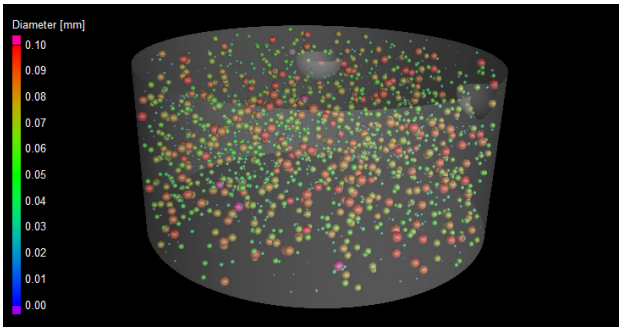

Figure 1. Digital porosity twin: Ø 3.8 mm, 1% porosity.

of the pores were drawn from a log-normal distribution (random.lognormvariate, μ = - 2.2, σ = 1.5 output in mm) within the limits [0.2, 50] µm, which was derived from high-resolution experimental data, until a porosity of 1 % was reached. The porosity was defined higher than experimentally observed to increase the number of defects, i.e. improve statistics. The pore positions were sampled uniformly inside the cylindrical volume and redrawn in case of overlap.

2.2. XCT simulation and analysis

The radiographic simulator aRTist 2.0 (BAM [14]) was used to model the employed XCT system [15]. Different levels of simplification, shown in Table 1, were used to model a range from ideal (#1) to realistic (#4). The detector model (#3-#4) was created using the DetectorCalc module that incorporates experimentally determined image noise and information about the scintillator. The pixel matrix consisted of 2048 px x 1440 px with a pitch of 0.2 mm. The finite focal spot (#4) was modelled as a 2D-Gaussian intensity distribution with a FWHM = 4.0 µm. 10 points were randomly sampled from this distribution and used for ray tracing. 1500 radiographs were simulated on an ideal circular trajectory and reconstructed with a voxel size of 2 µm using CERA 5.1 (Siemens).

Data analysis was performed in VG Studio MAX 3.4 (Volume Graphics). The object was segmented using the advanced surface determination algorithm and registered using the cylinder axis and the two calottes to create a datum system. Furthermore, a 3x3x3 median filter was applied to the volume data of simulation #4 (referred to as #4f). Subsequently, a porosity analysis was performed using the VGEasyPore module with sub-voxel accuracy, a relative threshold of 50 % and an area size of 10 voxel to determine the local contrast. To render the algorithm less prone to noise, defects were filtered with a probability threshold (non-disclosed quality metric) of 1 % and minimum defect size of 4 voxel, representing an equivalent radius of 2 µm. The following parameters were derived from the pore volume and surface area. The equivalent radius

$$r_{eq} = \left(\frac{3}{4\pi} V_{\text{defect}}\right)^{\frac{1}{3}}$$

and the sphericity that indicates the ratio between the surface area of an ideal sphere with the same volume as the defect and the surface area of the defect:

$$S = \frac{(36\pi V_{\text{defect}})^{\frac{1}{3}}}{A_{\text{defect}}}$$

2.3. Simulation results and discussion

Figure 2 shows simulated XCT slices under the four scenarios described in Table 1: (a) shows a very homogeneous grey value distribution with weak cone beam artefacts. In (b) the polychromatic X-ray spectrum causes beam hardening that results in a grey value gradient across the sample. For (c) detector noise was added that mainly results in form deviations of the defects (as indicated by the arrow). For scenario (d), a finite X-ray focal spot was simulated that causes blur due to the penumbra effect, which renders the contrast of small pores too weak to be detected using a threshold method. The arrow indicates a pore that was not detected by the algorithm.

To quantify the results, tables of the defects were exported from VG Studio MAX and compared to the reference file, which was used to create the digital porosity representation. By assigning the reference defects to the ones detected, comparisons can be made for each defect. As shown in Table 2, adding more error sources to the XCT simulation lowered the

Table 1. Simulated scenarios.

#	Focal spot	X-ray spectrum	Detector
1	point source	monochromatic (55 kV)	Ideal
2	point source	polychromatic, (100 kV, 0.1 mm Cu)	Ideal
3	point source	polychromatic, (100 kV, 0.1 mm Cu)	noise, energy sensitive
4	Gaussian, FWHM = 4 µm	polychromatic, (100 kV, 0.1 mm Cu)	noise, energy sensitive

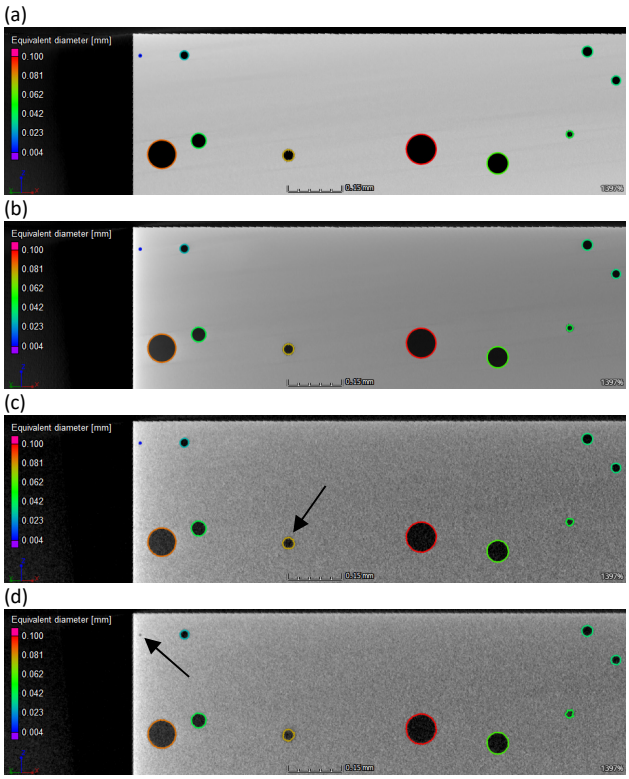

Figure 2. Simulated XCT slices for the different scenarios #1 (a) - #4 (d) shown in Table 1. Detected pores are outlined and colour coded according to their equivalent diameter. The arrows in (c) and (d), respectively, indicate a pore with a distorted shape and a pore, which was not detected due to the limited resolution.

Table 2. Global porosity evaluation results. The different simulation conditions are shown in Table 1.

#	Number of pores detected	Relative error	Porosity (%)	Relative error
Ref.	1813	-	1.0013	-
1	1767	-2.5 %	1.0005	-0.1 %
2	1755	-3.2 %	0.9334	-6.8 %
3	1758	-3.0 %	0.9569	-4.4 %
4	1722	-5.0 %	0.9776	-2.4 %
4f	1622	-10.5 %	0.8876	-10.4 %

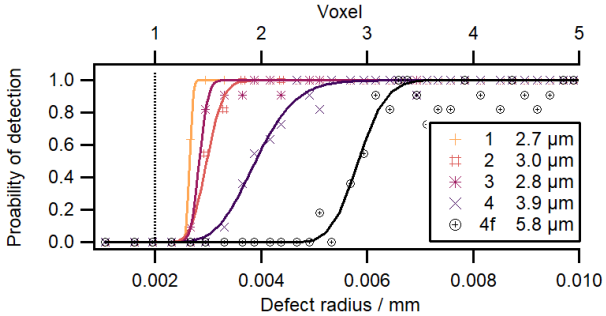

Figure 3. Simulated probability of detection (POD) for the scenarios described in Table 1. The dashed vertical line indicates the analysis threshold (#4f equal to #4 but data filtered with a 3x3x3 median filter).

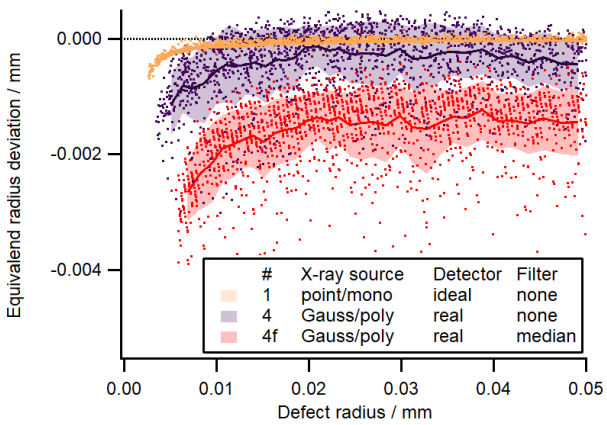

Figure 4. Simulated deviation of the equivalent radius.

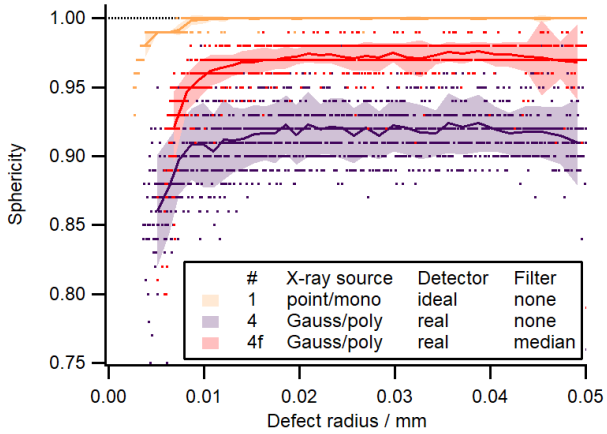

Figure 5. Simulated deviation of the sphericity (reference sphericity = 1).

number of detected pores and influenced the total porosity estimation. To investigate this effect further, a probability of detection (POD) analysis was performed [13], which is shown in Figure 3. With a point X-ray source (#1-#3) the minimum detectable defect radius was approximately 1.5 voxel (3 µm) and thus only slightly above the resolution limit. With a finite source size (#4), the minimum detectable defect radius increased to about the FWHM of the Gaussian X-ray source intensity distribution (4 µm). This was further increased to 3 voxel (6 µm) when applying a 3x3x3 median filter (#4f).

Next, the deviations of the equivalent radii of the defects were studied in dependence of defect size. In the ideal simulation (#1) the deviations showed a tendency to increase with smaller defect radii (Figure 4). This was also observed in the more realistic simulation (#4), however, the random scatter by the noise influence dominated. Filtering the XCT data (#4f) added a systematic deviation to the equivalent radii. For the shape factor sphericity (Figure 5), negligible deviations were observed for defects larger than 10 voxel in the ideal case (#1). Below, the shape of the defects was influenced by the finite voxel size. Adding noise and a finite X-ray focal spot (#4) led to a reduced sphericity, which was partially counteracted by median filtering (#4f). The deviations between reference and simulated values can be used as a basis for an uncertainty estimation [12].

3. Experimental porosity measurements

3.1. AM process

Small cylindrical Ti-6Al-4V samples with a diameter of 2 mm were manufactured using an custom-developed electron beam melting machine consisting of an Arcam S12 (vacuum chamber, powder management, build tank) retrofitted with an electron gun (pro beam AG & CO) with a maximum power of 6 kW and 60 kV accelerating voltage. To ensure occurrence of defects, the melting was performed using an electron beam power of 1.2 kW and a scanning speed of 8 ms^{-1} resulting in an energy input outside the optimal processing window.

3.2. XCT measurement and analysis

Measurements were performed on our custom metrology XCT system [15] at an acceleration voltage of 120 kV, a target power of 6 W using a 0.1 mm copper filter. The nominal focal spot size was 3 µm. 2000 projections with an exposure time of 5.3 s were recorded on a circular scan trajectory at a magnification of 127 and reconstructed with a voxel size of 1.6 µm.

To evaluate the porosity of the test cylinder we adhered to the following procedure: First, to exclude any influence from surface roughness, a cylindrical region of interest with a height of 1 mm and diameter of 1.1 mm was defined for analysis. Next, a 3x3x3 voxel median filter was applied to reduce noise. Subsequently, the porosity analysis described in section 2.2 was performed.

3.3. Experimental results and discussion

The results show a heterogeneous distribution of defects in terms of size (Figure 6) and shape (Figure 7). This suggests that the digital porosity twin requires refinement concerning the complexity of the defect shapes. In total, 476 defects were detected resulting in a porosity of 0.37 %. It can be seen that spherical air pores (Figure 7, red-orange) can be distinguished from high-aspect-ratio lack-of-fusion defects (Figure 7, green-blue) solely by their sphericity. As shown in Figure 8, a size dependent measurement uncertainty was assigned to each defect based on the simulation results in section 2.3. The presence of defects below the 50 % probability of detection (POD) threshold in Figure 8 is attributed to the uncorrected systematic underestimation of pore equivalent radii (Figure 4).

4. Conclusion

Digital porosity representations make it possible to study stochastic, e.g. detector noise, and local, e.g. beam hardening, influences on XCT porosity measurements.

Both the XCT simulation and the digital porosity twin require further refinement. The former by the introduction of e.g. machine geometry errors, in-line phase contrast and non-ideal detector pixels, the latter by better reflecting differently shaped defects, such as air pores and lack-of-fusion defects. This information could be deduced from higher resolution scan data.

The method enables benchmarking different segmentation and post-processing procedures to assess porosity against ground truth and deriving lower order models to predict the probability of detection solely based on a small number of parameters such as voxel size and focal spot. Next, the information gained from the digital representation can be fed back to correct the measured data for systematic errors, rendering it a full digital twin.

Acknowledgments

We thank Sylvain Hauser for XCT measurements and Federico Grasso Toro for fruitful discussions on digitalisation.

The project MANUELA has received funding from the European Union's Horizon 2020 research and innovation programme under grant agreement n°820774

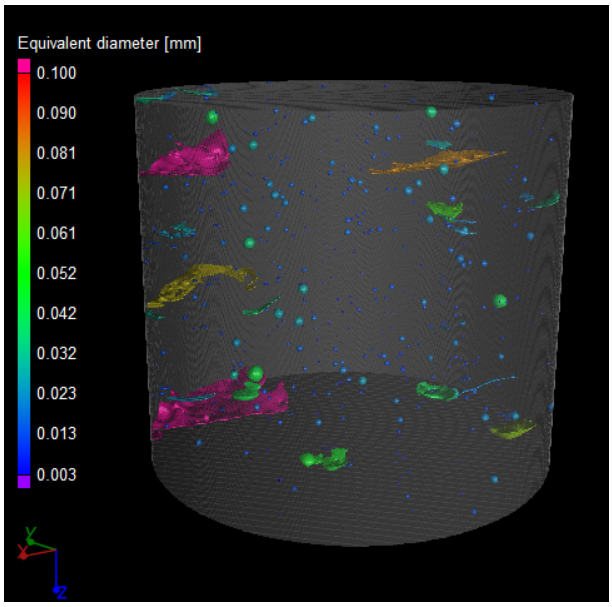

Figure 6. Experimentally determined defect equivalent diameter.

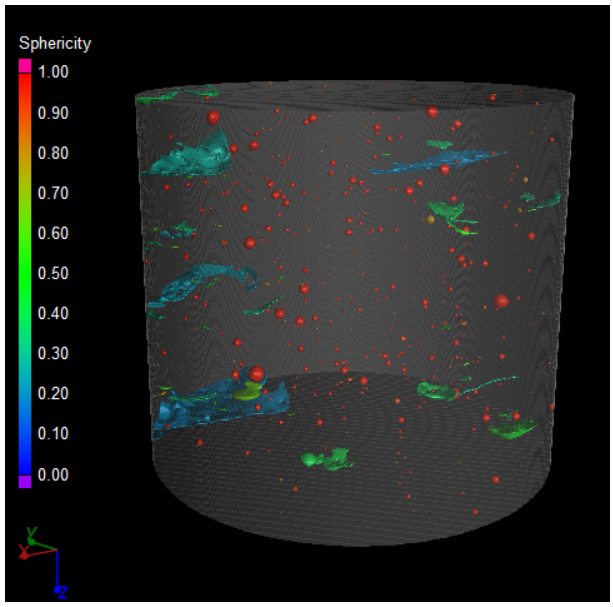

Figure 7. Experimentally determined defect sphericity.

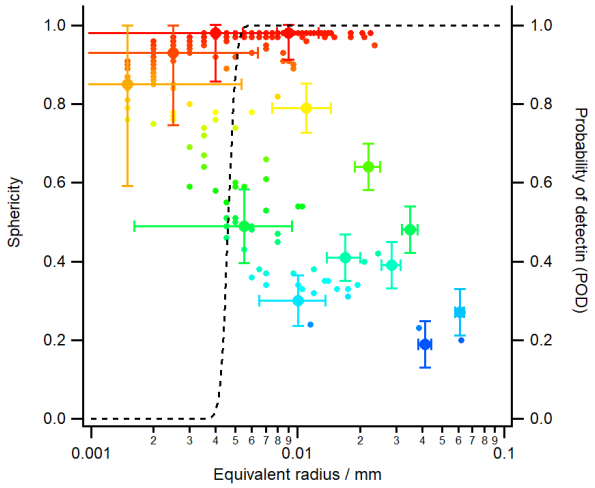

Figure 8. Experimentally determined defect sphericity versus equivalent radii. The error bars (only shown for a selection of markers) indicate the expanded measurement uncertainty (k=2) and the dashed line indicates the probability of detection derived from simulations.

References

[1] Leach R K, Bourell D, Carmignato S, Donmez A, Senin N and Dewulf W 2019 Geometrical metrology for metal additive manufacturing *CIRP Ann.* **68** 677–700

[2] Kruth J P, Bartscher M, Carmignato S, Schmitt R, De Chiffre L and Weckenmann A 2011 Computed tomography for dimensional metrology *CIRP Ann. - Manuf. Technol.* **60** 821–42

[3] du Plessis A, le Roux S G, Waller J, Sperling P, Achilles N, Beerlink A, Métayer J F, Sinico M, Probst G, Dewulf W, Bittner F, Endres H J, Willner M, Drégelyi-Kiss Á, Zikmund T, Laznovsky J, Kaiser J, Pinter P, Dietrich S, Lopez E, Fitzek O and Konrad P 2019 Laboratory X-ray tomography for metal additive manufacturing: Round robin test *Addit. Manuf.* **30** 100837

[4] Townsend A, Racasan R, Leach R, Senin N, Thompson A, Ramsey A, Bate D, Woolliams P, Brown S and Blunt L 2018 An interlaboratory comparison of X-ray computed tomography measurement for texture and dimensional characterisation of additively manufactured parts *Addit. Manuf.* **23** 422–32

[5] Sinico M, Ametova E, Witvrouw A and Dewulf W 2018 Characterization of Am Metal Powder With an Industrial Microfocus CT: Potential and Limitations *ASPE and euspen Summer Topical Meeting - Advancing Precision in Additive Manufacturing* (Lawrence Berkeley National Laboratory, Berkeley, California, USA) pp 1–6

[6] Bircher B A, Meli F, Küng A and Thalmann R 2018 A geometry measurement system for a dimensional cone-beam CT *8th Conference on Industrial Computed Tomography, Wels, Austria (iCT 2018)*

[7] Hermanek P, Zanini F and Carmignato S 2019 Traceable Porosity Measurements in Industrial Components Using X-Ray Computed Tomography *J. Manuf. Sci. Eng. Trans. ASME* **141**

[8] Verein Deutscher Ingenieure 2013 *VDI/VDE 2630 - 2.1 Coputertomografie in der dimensionellen Messtechnik: Bestimmung der Messunsicherheit und der Prüfprozesseignung von Koordinatenmessgeräten mit CT-Sensoren*

[9] Chen X, Zhang Q, Sun W, Zeng W, Jin X, Scott P J, Jiang X and Lou S 2020 Development of virtual reference samples for XCT measurements of additively manufactured surface texture Development of virtual reference samples for XCT measurements of additively manufactured surface texture *10th Conference on Industrial Computed Tomography* (Wels, Austria (iCT 2020))

[10] Yildiz E, Møller C and Bilberg A 2020 Virtual factory: Digital twin based integrated factory simulations *Procedia CIRP* **93** 216–21

[11] Riesener M, Schuh G, Dölle C and Tönnes C 2019 The digital shadow as enabler for data analytics in product life cycle management *Procedia CIRP* **80** 729–34

[12] Wohlgemuth F, Müller A M and Hausotte T 2018 Development of a virtual metrological CT for numerical measurement uncertainty determination using aRTist 2 *tm - Tech. Mess.* **85** 728–37

[13] Gollwitzer C, Bellon C, Deresch A, Baron H-U and Ewert U 2012 Reliability Investigations of Radiographic Testing Using aRTist as a Simulation Tool aRTist and SimuPOD *18th World Conference on Nondestructive Testing* (Durban, South Africa) pp 16–20

[14] Bellon C, Deresch A, Gollwitzer C and Jaenisch G-R 2012 Radiographic Simulator aRTist : Version 2 *18th World Conference on Nondestructive Testing* (Durban, South Africa)

[15] Bircher B A, Meli F, Küng A and Thalmann R 2020 METAS-CT: Metrological X-ray computed tomography at sub-micrometre precision *euspen's 20th International Conference & Exhibition* (Geneva, Switzerland (virtual))